Scripta Materialia 152 (2018) 49–54

Contents lists available at ScienceDirect

Scripta Materialia

journal homepage: www.elsevier.com/locate/scriptamat

Regular article

The influence of potassium content on octahedral-tilt disorder in $Na_{0.5}Bi_{0.5}TiO_3$-solid solutions near morphotropic phase boundary

Alexandra Neagu, Cheuk-Wai Tai *

Department of Materials and Environmental Chemistry, Stockholm University, SE-106 91 Stockholm, Sweden

ARTICLE INFO

Article history:
Received 9 March 2018
Accepted 9 April 2018
Available online xxxx

Keywords:
Electron scattering
Diffuse scattering
Transmission electron microscopy (TEM)
Perovskite
Ferroelectric ceramics

ABSTRACT

A semi-quantitative comparison of 3D electron diffraction data revealed structural differences at the nanoscale for three (95-*x*)$Na_{0.5}Bi_{0.5}TiO_3$-*x*$K_{0.5}Bi_{0.5}TiO_3$-5$BaTiO_3$ solid solutions close to the morphotropic phase boundary, with $x = 0, 5, 10$. Using a novel rotation electron diffraction technique, diffuse scattering intensity was recorded in 3D as continuous rods along *hk0.5* reciprocal-planes. By analyzing the different superstructure reflections and the intensity/morphology of diffuse scattering, a structural model of the local octahedral-tilt disorder for the different ceramics was developed. A good agreement was obtained between the experimental and simulated data with a model comprising of antiphase ($a^-a^-a^-$) and plate-like in-phase ($a^0a^0c^+$) nanodomains.

Since its discovery in the 1960s [1] $Na_{0.5}Bi_{0.5}TiO_3$ (NBT) and its solid solutions with $BaTiO_3$ (BT) and $K_{0.5}Bi_{0.5}TiO_3$ (KBT) have been intensively studied due to their potential applications as environmentally friendly piezoceramics [2,3]. NBT is a perovskite ferroelectric with high Curie temperature ~320 °C, high remnant polarization ~38 μC/cm^2 and large piezoelectric coefficient ~73 pC/N. The major drawbacks are the low depolarization temperature (T_d ~ 200 °C) and high coercive field (above 50 kV/cm) [4,5] which hinder the use of NBT in practical applications. In order to tackle these problems the focus has shifted towards solid solutions near the morphotropic phase boundary (MPB), such as NBT-*x*BT [6,7], NBT-*x*KBT [8] and NBT-*x*KBT-*y*BT [9,10], which exhibit enhanced electromechanical properties while maintaining a relatively high T_d.

NBT has been the topic of a large number of structural investigations [11–21]. Local structural deviations like cation displacements, short-range chemical order and oxygen octahedra tilting at the nanoscale play a crucial role in understanding the structure-property relationship. At room temperature the average structure of NBT has been described either by a rhombohedral (*R*3*c*) symmetry [22] with $a^-a^-a^-$ tilt system or monoclinic (*Cc*) symmetry [23,24] with $a^-a^-c^-$. Moreover, an additional tetragonal phase (*P*4*bm*) with in-phase $a^0a^0c^+$ tilting at nanoscale has been revealed by transmission electron microscopy (TEM) [13,15]. Another model suggests a single-phase continuous octahedral tilting ($a^-a^-c^+$) [16]. For NBT-solid solutions near/at the MPB, determining the type of octahedral-tilt becomes even more difficult due to the coexistence of different symmetries. Several previous studies focusing on the local structure in NBT-*x*BT [25–27] and NBT-*x*KBT [28,29] have also shown that nanoscale octahedral-tilt disorder is a characteristic feature of these materials. This implies that structural studies for NBT-based solid solutions near/at the MPB must go beyond the average structure and a deep understanding of the local oxygen octahedral tilting is needed.

In this work a novel rotation electron diffraction (RED) technique [30] was used to finely map the 3D reciprocal-space for three (95-*x*) $Na_{0.5}Bi_{0.5}TiO_3$-*x*$K_{0.5}Bi_{0.5}TiO_3$-5$BaTiO_3$ solid solutions near/at MPB, namely 95NBT-5BT, 90NBT-5KBT-5BT and 85NBT-10KBT-5BT. At the MPB a transition from a ferroelectric rhombohedral (*R*3*c*) phase to a ferroelectric tetragonal (*P*4*bm*) phase occurs for x ~ 6% in the case of NBT-*x*BT [6,7] and x ~ 5%/y ~ 5% in the case of NBT-*x*KBT-*y*BT [6,31]. From X-ray diffraction studies the average structure of 95NBT-5BT [32] was determined to be rhombohedral (*R*3*c*), 90NBT-5KBT-5BT [31,33] has a composition at the MPB with the average structure described as phase coexistence of rhombohedral (*R*3*c*) and tetragonal (*P*4*bm*) symmetries and 85NBT-10KBT-5BT [31] presents long-range tetragonal (*P*4*bm*) symmetry. By analyzing the intensity and morphology of superstructure reflections (SSRs) and diffuse scattering features in 3D a comprehensive model of the local octahedral-tilt disorder was developed.

The ceramic samples were synthesized by a mixed oxide route as described in detail in ref. [31]. The TEM specimens were prepared by ion milling (Fishicone Model 1050). The RED data, selected-area electron diffraction (SAED) patterns and centered dark-field (CDF) images were recorded at room temperature using a JEOL JEM-2100F microscope operated at 200 kV equipped with a Gatan Orius 200D CCD camera. A SAED aperture with an effective diameter of ~520 nm was used. All SAED patterns are shown in logarithmic scale and were processed in order to enhance the visibility of the weak SSRs. The RED

* Corresponding author.
E-mail address: cheuk-wai.tai@mmk.su.se (C.-W. Tai).

https://doi.org/10.1016/j.scriptamat.2018.04.016
1359-6462/

data collection was done using REDaquisition software [30]. This method combines mechanical goniometer tilting (±21° with a tilt-step of 2° along x direction) with very fine beam tilting (±1° with a tilt-step of 0.1°), and does not require exact zone axis (ZA) alignment. In total 440 diffraction patterns were recorded for each composition. The reconstruction of the 3D reciprocal-space volume was done using REDprocessing [30] while the 3D visualization was used Kitware VolView. The strong electron-matter interaction is an advantage in this case since both SSRs and diffuse scattering intensity are very weak. DISCUS [34] was used to build the models for local structural disorder and to calculate electron diffraction patterns along the *hk0.5* reciprocal-plane based on the kinematical approximation. The final patterns were obtained after averaging the results from 20 different simulations, in order to reduce the anisotropic diffraction intensities. The initial supercell was 50 × 50 × 50 unit cells with space group *Pm*-3 *m* (a = 3.8894 Å). A more detailed account of the simulation procedure can be found in ref. [35].

In Fig. 1(a–c) SAED patterns recorded along the $[112]_{pc}$ zone axis (ZA) are shown for (a) 95NBT-5BT, (b) 95NBT-5KBT-5BT and (c) 85NBT-10KBT-5BT ceramics. For simplicity and convenience of comparison, pseudocubic unit cell (*Pm*-3*m*) was used for indexing. Two types of SSRs are simultaneously observed namely, ½(*ooo*) and ½(*ooe*) as depicted by the circles in Fig. 1(a–c). This indicates a coexistence of two oxygen octahedra tilting systems, one antiphase $a^-a^-a^-$ and one in-phase $a^0a^0c^+$ respectively. Mixed tilting systems have been excluded as no ½(*oee*) SSRs [36] are observed. The diffraction patterns suffer from double diffraction so kinematically forbidden reflections like ½(11$\bar{1}$) and ½(1$\bar{1}$0) can be observed. In the case of $a^-a^-a^-$ the condition for allowed SSRs is $h \neq \pm k$, $k \neq \pm l$ and $l \neq \pm h$ while for $a^0a^0c^+$ the condition is $h \neq \pm k$ [37]. The insets in Fig. 1(a–c) show an enlarged view of the two types of SSRs and they reveal that for 95NBT-5BT ceramic ½(*ooo*) SSRs are stronger than the ½(*ooe*) ones while with K addition the relative intensity ratio is reversed. For 85NBT-10KBT-5BT ½(*ooe*) SSRs are stronger than the ½(*ooo*) ones. In the case of 90NBT-5KBT-5BT both ½(*ooo*) and ½(*ooe*) SSRs present comparable intensities. Although SAED patterns suffer from dynamical effects and thickness variations, which makes a quantitative analysis of intensities very difficult, the contribution to the scattering intensities is not dominant. Hence, the trend of intensity change for the two types of SSRs could be observed for different grains in the ceramics. However, it should be mentioned that only the SSRs intensities relatively to each other are compared in order to estimate the relative phase fractions of antiphase and in-phase tilted nanodomains [38,39]. These findings are in good agreement with the ceramics' average long-range structures [31–33].

All samples having both ½(*ooo*) and ½(*ooe*) SSRs indicates that the structure at the nanoscale deviates from the average one. For 90NBT-5BT the dominant octahedral tilt system is $a^-a^-a^-$ while for 85NBT-10KBT-5BT the one is $a^0a^0c^+$. Similar SSRs were previously reported for NBT [13,15] and other NBT-BT [40,41] and NBT-KBT-BT [42,43] near/at the MPB. This suggests that the coexistence of antiphase and in-phase tilted nanodomains is an intrinsic characteristic of (95-*x*) $Na_{0.5}Bi_{0.5}TiO_3$-*x*$K_{0.5}Bi_{0.5}TiO_3$-5$BaTiO_3$ solid solutions.

In order to visualize these nanodomains, CDF images of antiphase and in-phase nanodomains were recorded using the ½(*ooo*) and ½(*ooe*) SSRs. The antiphase domains (Fig. 2(a–c)) were recorded close to $[011]_{pc}$ ZA while the in-phase domains (Fig. 2(d–f)) were recorded close to either $[111]_{pc}$ or $[001]_{pc}$ ZAs. The bright contrast in the images represents the tilted regions which scatter the electrons into the selected ½(*ooo*) or ½(*ooe*) SSRs. On the other hand, the dark contrast corresponds to regions with octahedral tilting about a different axis than the antiphase/in-phase tilting and/or regions with no octahedral tilting. The distribution of antiphase and in-phase nanodomains is rather uniform but a direct correlation between the macroscopic ferroelectric domains (Supplementary Fig. 1) and the antiphase/in-phase nanodomains was not found. Therefore, the octahedral tilted nanodomains do not follow the long-range ferroelectric order. The difficulty in assigning a long-range octahedral-tilt system for NBT-solid solutions near/at the MPB might be attributed to the fact that antiphase and in-phase nanodomains intimately coexist at the nanoscale and the long-range octahedral tilting is disturbed. Similar results were previously reported for NBT-based ceramics with compositions near the MPB [42,44]. The sizes of the octahedral tilted domains were measured in the CDF images. It is found that in average ~2–5 nm for antiphase nanodomains for all compositions. In the case of in-phase nanodomains we observed slight differences for the three compositions: ~2–3 nm for 95NBT-5BT, ~2–6 nm for 90NBT-5KBT-5BT and ~2–7 nm for 85NBT-10KBT-5BT. This information was used as a starting point for the simulation of local octahedral-tilt disorders.

In order to investigate how the nanoscale octahedral-tilt disorder changes with K addition electron diffuse scattering data was recorded in 3D using the RED method. In Fig. 3a the entire reciprocal-space volume projected along $[001]_{pc}$ direction, for 90NBT-5KBT-5BT ceramic, is shown. The *hk0.5*-plane is depicted by a yellow dashed line. The experimental *hk0.5*-planes cut from the 3D RED reciprocal-space volumes recorded for the different ceramics are shown in Fig. 3(b–d). Due to the limited tilting-range (±21°) only parts of the *hk0.5*-slices were recorded. The initial orientation is different for each grain which means that different regions in the reciprocal-space were mapped for each composition. A careful analysis of the 3D RED data revealed that

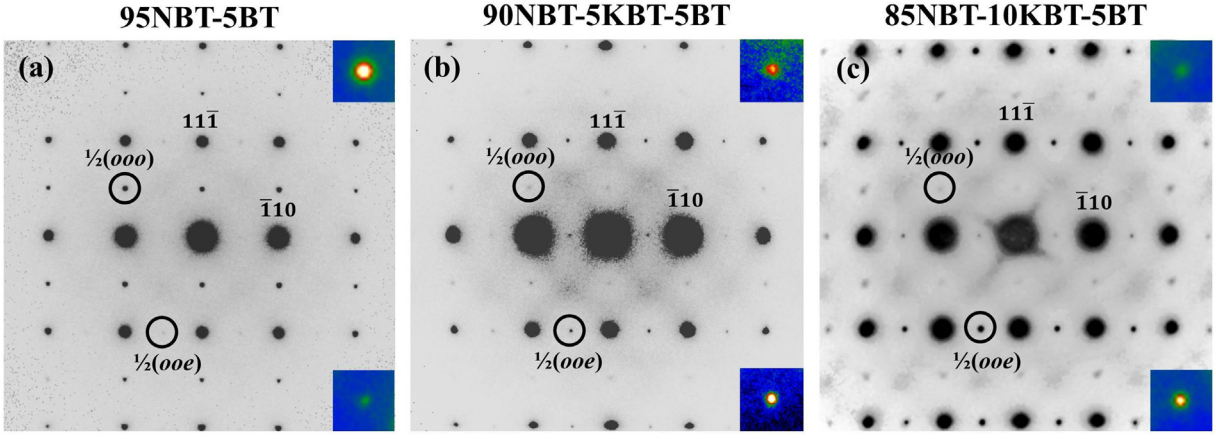

Fig. 1. SAED patterns recorded along $[112]_{pc}$ ZA for (a) 95NBT-5BT, (b) 90NBT-5KBT-5BT and (c) 85NBT-10KBT-5BT ceramics. The insets in (a), (b) and (c) show an enlarged view of the SSRs depicted by black circles. The inset in the upper-right corner of a diffraction pattern shows the ½(*ooo*) SSRs while the inset in the lower-right corner shows the ½(*ooe*) SSRs.